Accelerating Relativistic Exact-Two-Component Density Functional Theory Calculations with Graphical Processing Units

Mikael Kovtun,[†,¶] Eleftherios Lambros,[*,†,¶] Aodong Liu,[†] Diandong Tang,[†]

David B. Williams-Young,[*,‡] and Xiaosong Li[*,†]

†*Department of Chemistry, University of Washington*

Seattle, Washington 98115, United States

‡*Applied Mathematics and Computational Research Division*

Lawrence Berkeley National Laboratory

Berkeley, California 94720, United States

¶*These authors contributed equally to this work*

E-mail: elambros@uw.edu; dbwy@lbl.gov; xsli@uw.edu

Abstract

Numerical integration of the exchange-correlation potential is an inherently parallel problem that can be significantly accelerated by graphical processing units (GPUs). In this letter, we present the first implementation of GPU-accelerated exchange-correlation potential in the GauXC library for relativistic, two-component density functional theory. By benchmarking against copper, silver, and gold coinage metal clusters, we demonstrate the speed and efficiency of our implementation, achieving significant speedup compared to CPU-based calculations. One GPU card provides computational power equivalent to roughly 400 CPU cores in the context of this work. The speedup

further increases for larger systems, highlighting the potential of our approach for future, more computationally demanding simulations. Our implementation supports arbitrary angular momentum basis functions, enabling the simulation of systems with heavy elements and providing substantial speedup to relativistic electronic structure calculations. This advancement paves the way for more efficient and extensive computational studies in the field of density functional theory.

Recently, there has been a resurgence of interest to develop and rationally design materials that exploit the properties of electronic spin.[1–5] Applications for these materials range from functional magnetic materials[6–8] and quantum computing,[9] to spintronic devices[3,10,11] and catalytic active sites.[12,13] Fundamental to these technological advances are the important physical characteristics of electronic spin and spin-couplings.[9,14,15] As such, there is a strong need to develop theoretical methods which properly describe electronic spin and spin interactions in materials, as well as the computational capability to simulate the large systems where such phenomena manifest.

From a theoretical perspective, a rigorous description of electronic spin and its interactions is fundamentally rooted in relativistic quantum mechanics. This theory uses the Dirac equation to obtain the relativistic wavefunction in place of the non-relativistic Schrödinger equation.[16–20] Here, the wavefunction is represented using 4-vectors, also known as 4-component bispinors. These structures represent the electronic wavefunction using small and large components, and allows the wavefunction to have positive and negative energy eigenstates.

Spin is inherently encoded into this wavefunction through the α and β components of the spinor. In practice though, using 4-component representations of relativistic wavefunctions is computationally cumbersome, requiring additional storage and computational throughput than corresponding non-relativistic calculations. Furthermore, most chemically-relevant problems, such as spin-forbidden transitions, spin-orbit coupling, and the inert-pair effect,[21–24] do not require an explicit treatment within the 4-component framework. It is of-

ten advantageous from a practical point of view to transform the 4-component Hamiltonian into an electron-only effective 2-component form. This is known as a 2-component transformation, which uses unitary operators to fold the small component of the wavefunction into a pseudo-large component form.[25–32]

Electronic structure methods developed within the 4- or 2-component Dirac framework do not treat spin as a good quantum number, *i.e.*, the spin angular momentum is no longer aligned in a single axis. This approach requires maintaining electronic properties in their four-current form or as a complete magnetization vector.[14] Because the spin-orbit operator interacts with the entire angular momentum tensor, all three components of the magnetic density (ρ_x, ρ_y, ρ_z) must be incorporated in the calculations, leading to a significant increase in computational cost compared to non-relativistic one-component calculations.

Relativistic density functional theory (DFT)[33–35] encompasses a powerful set of low-cost theoretical tools that can be used to investigate spin-driven chemical and materials processes and properties at large and experimentally relevant scales. Practical applications commonly utilize workhorse methods implemented in the relativistic 2-component and 4-component Kohn-Sham formalism.[36] While the exact functional is unknown, the excellent balance between accuracy and computational cost makes density functional approximations particularly popular for tackling problems in a wide array of contexts, from physical chemistry and material science[11,37–39] all the way to biochemistry and structural biology.[40,41] Many popular software packages that implement relativistic density functional theory leverage the latest advances in high performance computing in order to further accelerate calculations, making larger and more complex systems accessible to this theory.[4,42–46]

In DFT, the evaluation of the exchange-correlation energy and potential is performed using a numerical integration scheme.[47–49] This numerical integration procedure is highly amenable to parallelization since the integrand of the functional only depends on the density and density gradients at each point. Furthermore, efficient algorithms for integrating the exchange-correlation potential in non-collinear relativistic DFT have been developed for cen-

tral processing unit (CPU)-based systems.[50–60] Similarly, graphics processing units (GPU) have long been used to perform the numerical integration for the exchange-correlation potential in *non-relativistic* density functional theory, and have been shown to provide significant speedup over CPU based numerical integration schemes.[61–64] As the computation of the exchange-correlation potential is done at every step of self-consistent field and real-time time-dependent calculations[65–69] a software paradigm that prioritizes speed and concurrency is highly desirable.

Despite the clear advantage of GPUs for usage in density functional calculations, to the authors' best knowledge, this hardware has not yet been leveraged to perform fully non-collinear relativistic calculations. In this work, we exploit GPU acceleration in relativistic quantum chemistry calculations. We showcase a GPU implementation of the highly efficient 2-component relativistic DFT integration algorithm and benchmark its performance evaluating large coinage metal nanoparticles against the corresponding CPU implementation. The results presented in this letter demonstrate how GPUs can be used to heavily accelerate relativistic DFT calculations.

The GPU implementation of non-collinear relativistic DFT is developed within the exact-two-component (X2C) relativistic framework.[27–32,55,70–85] In X2C, one electron spin-orbit coupling is included variationally during the optimization of molecular spinor orbitals. Two-electron spin-orbit effects are accounted for by an empirical screened nuclear spin-orbit (SNSO) treatment.[84,86]

Due to the spinor nature of molecular orbitals (MOs) in relativistic calculations, the Kohn-Sham and density matrices ($\mathbf{F}$ and $\mathbf{P}$) formally have the spin-blocked structure

$$\mathbf{X} = \begin{bmatrix} \mathbf{X}^{\alpha\alpha} & \mathbf{X}^{\alpha\beta} \\ \mathbf{X}^{\beta\alpha} & \mathbf{X}^{\beta\beta} \end{bmatrix}, \quad \mathbf{X} \in \{\mathbf{F}, \mathbf{P}\}, \tag{1}$$

with

$$P^{\zeta\zeta'}_{\mu\nu} = \sum_i C^{\zeta}_{\mu i} C^{\zeta' *}_{\nu i}, \qquad \zeta, \zeta' \in \{\alpha, \beta\} \tag{2}$$

where $\mathbf{C}$ is the MO coefficient matrix and $\{\mu, \nu\}$ are indices for atomic orbital bases. We cast the rank–2 spinor structure of $\mathbf{F}$ and $\mathbf{P}$ into the Pauli quaternion form

$$\mathbf{F} = \mathbf{F}^S \otimes \mathbf{I}_2 + \sum_{k\in\{x,y,z\}} \mathbf{F}^k \otimes \boldsymbol{\sigma}_k \tag{3}$$

$$\mathbf{P} = \mathbf{P}^S \otimes \mathbf{I}_2 + \sum_{k\in\{x,y,z\}} \mathbf{P}^k \otimes \boldsymbol{\sigma}_k \tag{4}$$

which gives rise to an exchange-correlation potential in the quaternion structure $\{\mathbf{V}^S_{\rm xc}, \mathbf{V}^z_{\rm xc}, \mathbf{V}^y_{\rm xc}, \mathbf{V}^x_{\rm xc}\}$, defined as

$$V^S_{{\rm xc},\mu\nu} = \frac{\delta E_{\rm xc}}{\delta P^S_{\mu\nu}}, \quad V^x_{{\rm xc},\mu\nu} = \frac{\delta E_{\rm xc}}{\delta P^x_{\mu\nu}}, \quad V^y_{{\rm xc},\mu\nu} = \frac{\delta E_{\rm xc}}{\delta P^y_{\mu\nu}}, \quad V^z_{{\rm xc},\mu\nu} = \frac{\delta E_{\rm xc}}{\delta P^z_{\mu\nu}} \tag{5}$$

The reader is referred to Ref. 56 for more details on the integration and assembly of the $V_{\rm xc}$ terms of the Kohn–Sham Fock matrix using a quaternion formalism. In this work, we leverage the parallelized computing capability of GPUs to perform the integration in Eq. (5). Integration points are batched together to maximize cache utilization and memory contiguity.[56,61]

The X2C DFT method on the GPUs presented in this work is made publicly available via the GauXC[56,87,88] library for exascale Gaussian basis DFT. All numerical results in this study were obtained using GauXC evaluating density matrices generated by ChronusQ,[89] carried out on the HYAK cluster at the University of Washington. A single A100 GPU card was used for the benchmark study. Details of the implementation are provided in the Supporting Information.

We assessed the computational performance of our GPU implementation through all-electron X2C DFT calculations on metal nanoparticles, containing 20 to 40 atoms per cluster.

Table 1. Grid sizes per atom for the set of grid densities used in this work for Cu, Ag, and Au atoms.

Grid Name	N_{rad}	N_{ang}
`Fine`	75	302
`UltraFine`	99	590
`SuperFine`	250	974

Table 2. Number of basis functions (N_{bf}) per atom for the SAPPORO-DKH3 basis set used in this work for Cu, Ag, and Au atoms.

Basis Type	N_{bf} (Cu)	N_{bf} (Ag)	N_{bf} (Au)
`DZ`	56	65	81
`TZ`	94	103	119
`QZ`	141	150	166

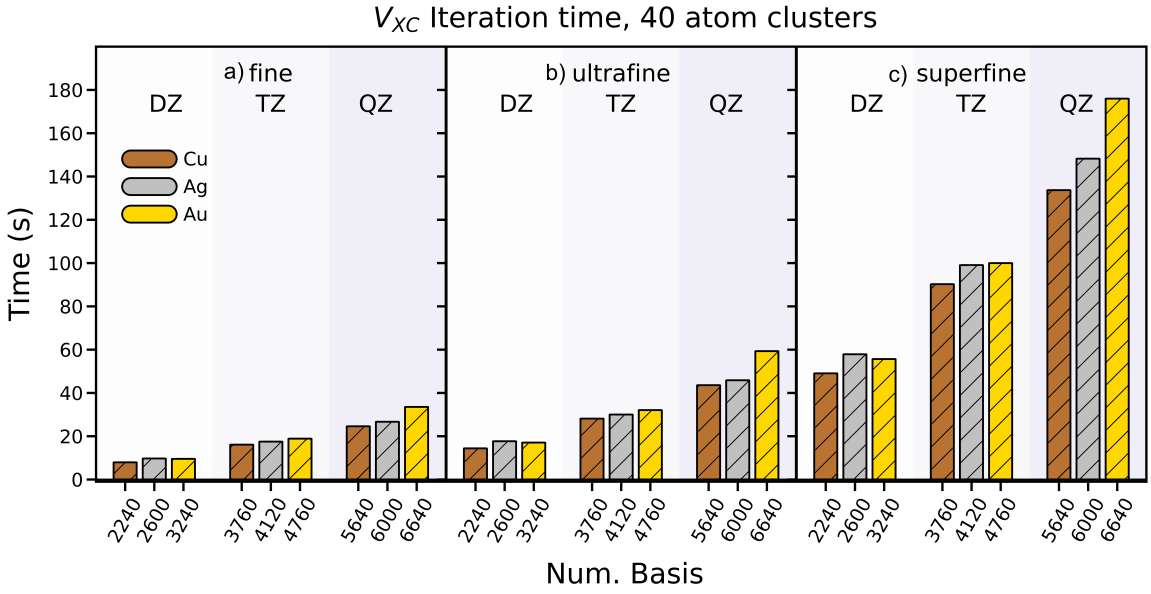

Figure 1. X2C V_{xc} computation times for Cu_{40}, Ag_{40}, and Au_{40} clusters for **a)** `Fine`, **b)** `Ultrafine`, **c)** `Superfine` grid sizes on an A100 GPU card using the SAPPORO-DKH3 DZ, TZ, and QZ basis sets. The numbers of basis functions for each cluster are indicated on the x-axis.

The metal cluster structures were generated using the NanoCrystal suite.[90–93] The setup of the grid and the selection of basis functions are detailed in Table 1, Table 2, and Figure 1, respectively. These systems are the largest all-electron relativistic calculations performed to date. Our benchmark tests peaked with a calculation on a Au_{40} nanocluster, which consists of 6640 basis functions.

Figure 1 shows the V_{xc} integration times using the GPU based numerical integrator for X2C-PBE[94,95] Cu_{40}, Ag_{40}, and Au_{40} nanoparticles. The integration times are plotted over the three different basis sets and three different integration grids. For the `Fine` grid in Figure 1.a, all metals display numerical integration times of less than ∼40s irrespective of the basis set. The `UltraFine` grid shows increased integration times, from ∼20s with the DZ basis to ∼60s with the QZ basis. The `SuperFine` grid is the most computationally expensive with integration times of ∼60s with the DZ basis and up to ∼180s with the QZ basis. For relativistic DFT calculations, the `SuperFine` grid is recommended to reliably produce spin and spin-orbit properties on the order of millielectron volts (meV). The timing results in this figure indicate roughly linear scaling with number of basis functions and grid points for all coinage metal clusters. Similar scaling results are observed for smaller clusters.

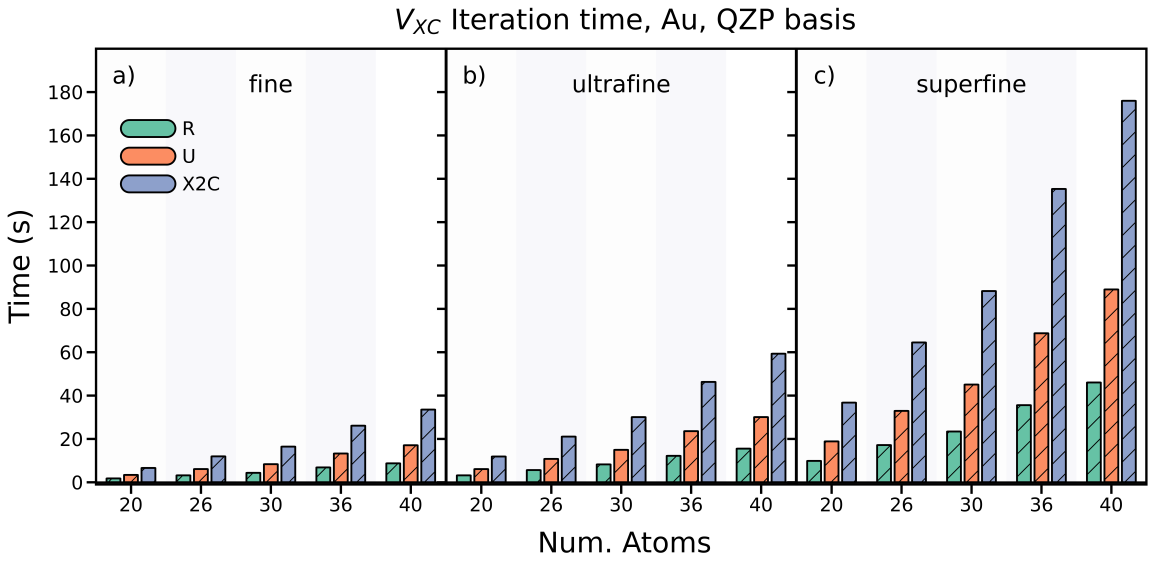

Figure 2. Comparison of V_{xc} computation times for Au clusters using restricted, unrestricted, and X2C schemes for **a)** `Fine`, **b)** `Ultrafine`, **c)** `Superfine` grid sizes on an A100 GPU card using the SAPPORO-DKH3 QZ basis set.

The second analysis in this work, shown in Figure 2, plots the V_{xc} integration times for Au_{20-40} nanoparticles, calculated with the restricted, unrestricted, and X2C Kohn-Sham schemes on an A100 GPU. The integration times are plotted for three different integration grids using only the largest, QZ, basis. A complete set of corresponding figures spanning all three basis sets and metal identities is available in the supporting information. The `Fine` grid produces integration times between ∼5-40s and for all three schemes. With the `UltraFine` grid, X2C is shown to be roughly twice as expensive as an unrestricted Kohn-Sham integration, which in turn is twice as expensive as a restricted Kohn-Sham calculation. X2C integration times here are ∼10s for the Au_{20} cluster up to about ∼60s for the Au_{40} cluster. The `SuperFine` grid produces the longest computation times with ∼40s for Au_{20} to ∼180s for Au_{40}.

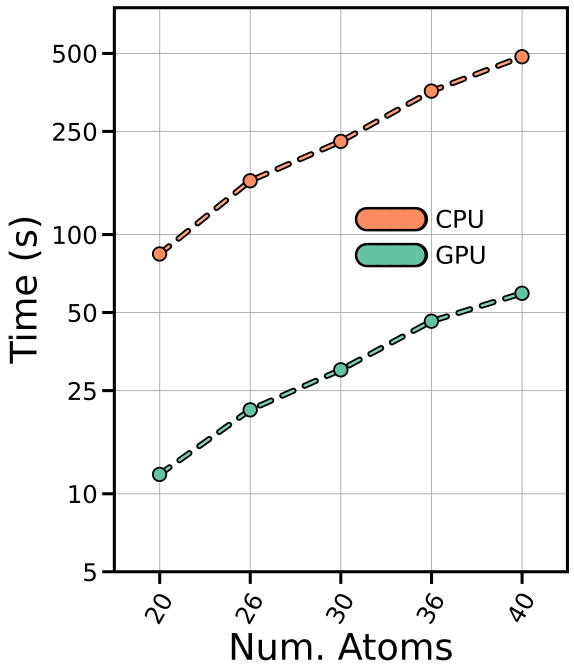

Figure 3. Comparison of V_{xc} computation times for Au clusters on a 40-core CPU node and an A100 GPU card, for Au clusters using the SAPPORO-DKH3 QZ basis and `UltraFine` grid.

Finally, in order to demonstrate the computational speedup of the GPU implementation relative to the corresponding CPU based scheme for calculating the exchange-correlation potential in GauXC, Figure 3 plots the time required to compute V_{xc} on an NVIDIA A100

GPU against the corresponding CPU implementation running on two Intel XEON Gold 6230 CPUs (total 40 cores) at 2.10GHz. This is performed on Au_{20} with 3320 basis functions up to Au_{40} with 6640 basis functions using the `UltraFine` grid and SAPPORO-DKH3 QZ basis set. Table S1 in the supporting information contains corresponding data spanning all grids and basis sets. Across the board for all examined cluster sizes, the GPU performs about $\sim$10$\times$ faster than the corresponding CPU implementation, with larger speedup for bigger systems. It should be emphasized here that MPI implementations are available for CPU and GPU numerical integration schemes, which could reduce the calculation time. Assuming linear scaling with number of CPU cores, it would take about 400 CPU cores to produce the same computation time as one A100 GPU card. This metric highlights the computational efficiency of the GPU implementation of X2C DFT substantial speedup can be achieved using a single GPU card on a single node, with increasing speedup for larger systems.

This Letter highlights the acceleration of non-collinear relativistic X2C DFT calculations by exploiting GPU hardware. This work showcases the exceptionally low integration times on a GPU for X2C calculations on coinage metal nanoclusters. The numerical integration takes between 10-60s for these systems on the GPU. We demonstrate a 10$\times$ speedup for V_{xc} calculations of coinage metal nanoparticles relative to a CPU implementation (one A100 vs. 40 CPU cores). It should be emphasized that the systems examined in this letter are large systems composed of many heavy transition metals. Our GPU implementation is able to handle arbitrary-order angular momentum basis functions, making it amenable to heavy element systems of interest to the materials and solid state chemistry fields.

Supporting Information Available

The supporting information includes additional comparisons of the V_{xc} computation times, the raw GPU and CPU computational times for Au clusters, as well as GPU implementation details.

Acknowledgements

This work is supported by the U.S. Department of Energy, Office of Science, Basic Energy Sciences, in the Computational and Theoretical program (Grant No. DE-SC0006863) for the development of the relativistic electronic structure and quantum field theory. The software infrastructure, including DFT integrator and self-consistent-field, is supported by the Office of Advanced Cyberinfrastructure, National Science Foundation (Grant No. OAC-2103717).

References

(1) Buchachenko, A. L.; Berdinsky, V. L. Electron Spin Catalysis. *Chem. Rev.* **2002**, *102*, 603–612.

(2) Awschalom, D. D.; Bassett, L. C.; Dzurak, A. S.; Hu, E. L.; Petta, J. R. Quantum Spintronics: Engineering and Manipulating Atom-Like Spins in Semiconductors. *Science* **2013**, *339*, 1174–1179.

(3) Feng, Y. P.; Shen, L.; Yang, M.; Wang, A.; Zeng, M.; Wu, Q.; Chintalapati, S.; Chang, C.-R. Prospects of Spintronics Based on 2D Materials. *Wiley Interdiscip. Rev. Comput. Mol. Sci.* **2017**, *7*, e1313.

(4) Prentice, J. C.; Aarons, J.; Womack, J. C.; Allen, A. E.; Andrinopoulos, L.; Anton, L.; Bell, R. A.; Bhandari, A.; Bramley, G. A.; Charlton, R. J., et al. The ONETEP Linear-Scaling Density Functional Theory Program. *J. Chem. Phys.* **2020**, *152*, 174111.

(5) Zhang, H. High-Throughput Design of Magnetic Materials. *Electron. Struct.* **2021**, *3*, 033001.

(6) Li, N.; Zhu, Z.; Chueh, C.-C.; Liu, H.; Peng, B.; Petrone, A.; Li, X.; Wang, L.; Jen, A. K.-Y. Mixed Cation $FA_xPEA_{1-x}PbI_3$ with Enhanced Phase and Ambient Stability toward High-Performance Perovskite Solar Cells. *Adv. Energy Mater.* **2016**, *7*, 1601307.

(7) Gary, D. C.; Petrone, A.; Li, X.; Cossairt, B. M. Investigating the Role of Amine in InP Nanocrystal Syntheses: Destabilizing Cluster Intermediates by Z-Type Ligand Displacement. *Chem. Commun.* **2017**, *53*, 161–164.

(8) Beck, R. A.; Lu, L.; Sushko, P. V.; Xu, X.; Li, X. Defect-Induced Magnetic Skyrmion in a Two-Dimensional Chromium Triiodide Monolayer. *JACS Au* **2021**, *1*, 1362–1367.

(9) Ladd, T. D.; Jelezko, F.; Laflamme, R.; Nakamura, Y.; Monroe, C.; O'Brien, J. L. Quantum Computers. *Nature* **2010**, *464*, 45–53.

(10) Petrone, A.; Goings, J. J.; Li, X. Quantum Confinement Effects on Optical Transitions in Nanodiamonds Containing Nitrogen Vacancies. *Phys. Rev. B* **2016**, *94*, 165402.

(11) Zhang, Y.; Cui, Z.; Sa, B.; Miao, N.; Zhou, J.; Sun, Z. Computational Design of Double Transition Metal MXenes With Intrinsic Magnetic Properties. *Nanoscale Horiz.* **2022**, *7*, 276–287.

(12) Hafner, J.; Wolverton, C.; Ceder, G. Toward Computational Materials Design: The Impact of Density Functional Theory on Materials Research. *Mr Bull.* **2006**, *31*, 659–668.

(13) Chen, B. W.; Xu, L.; Mavrikakis, M. Computational Methods in Heterogeneous Catalysis. *Chem. Rev.* **2020**, *121*, 1007–1048.

(14) Goings, J. J.; Egidi, F.; Li, X. Current Development of Non-collinear Electronic Structure Theory. *Int. J. Quant. Chem.* **2018**, *118*, e25398.

(15) Thiering, G.; Gali, A. Ab Initio Calculation of Spin-Orbit Coupling for an NV Center in Diamond Exhibiting Dynamic Jahn-Teller Effect. *Phys. Rev. B* **2017**, *96*, 081115.

(16) Srednicki, M. *Quantum Field Theory*; Cambridge University Press, 2007.

(17) Beresteckij, V. B.; Lifšic, E. M.; Pitaevskij, L. P.; Beresteckij, V. B.; Landau, L. D. *Quantum Electrodynamics*, 2nd ed.; Course of Theoretical Physics; Butterworth-Heinemann: Oxford, 2008.

(18) Faegri, K.; Dyall, K. *Introduction to Relativistic Quantum Chemistry*, 1st ed.; Oxford University Press, 2007.

(19) Reiher, M.; Wolf, A. *Relativistic Quantum Chemistry*, 2nd ed.; Wiley-VCH, 2015.

(20) Liu, W. *Handbook of Relativistic Quantum Chemistry*; Springer-Verlag Berlin Heidelberg, 2017.

(21) Capelle, K.; Vignale, G.; Ullrich, C. A. Spin Gaps and Spin-Flip Energies in Density-Functional Theory. *Phys. Rev. B* **2010**, *81*, 125114.

(22) Pyykkö, P. Relativistic Effects in Chemistry: More Common Than You Thought. *Annu. Rev. Phys. Chem.* **2012**, *63*, 45–64.

(23) Jacob, C. R.; Reiher, M. Spin in Density-Functional Theory. *Int. J. Quantum Chem.* **2012**, *112*, 3661–3684.

(24) Valentine, A. J. S.; Li, X. Intersystem Crossings in Late-Row Elements: A Perspective. *J. Phys. Chem. Lett.* **2022**, *13*, 3039–3046.

(25) Douglas, M.; Kroll, N. M. Quantum Electrodynamical Corrections to the Fine Structure of Helium. *Ann. Phys.* **1974**, *82*, 89–155.

(26) Hess, B. A. Relativistic Electronic-Structure Calculations Employing a Two-Component No-Pair Formalism With External-Field Projection Operators. *Phys. Rev. A* **1986**, *33*, 3742–3748.

(27) Dyall, K. G. Interfacing Relativistic and Nonrelativistic Methods. I. Normalized Elimination of the Small Component in the Modified Dirac Equation. *J. Chem. Phys.* **1997**, *106*, 9618–9626.

(28) Dyall, K. G. Interfacing Relativistic and Nonrelativistic Methods. II. Investigation of a Low-Order Approximation. *J. Chem. Phys.* **1998**, *109*, 4201–4208.

(29) Filatov, M.; Cremer, D. A New Quasi-Relativistic Approach for Density Functional Theory Based on the Normalized Elimination of the Small Component. *Chem. Phys. Lett.* **2002**, *351*, 259–266.

(30) Kutzelnigg, W.; Liu, W. Quasirelativistic Theory Equivalent to Fully Relativistic Theory. *J. Chem. Phys.* **2005**, *123*, 241102.

(31) Liu, W.; Peng, D. Infinite-Order Quasirelativistic Density Functional Method Based on the Exact Matrix Quasirelativistic Theory. *J. Chem. Phys.* **2006**, *125*, 044102.

(32) Ilias, M.; Saue, T. An Infinite-Order Relativistic Hamiltonian by a Simple One-Step Transformation. *J. Chem. Phys.* **2007**, *126*, 064102.

(33) Rajagopal, A.; Callaway, J. Inhomogeneous Electron Gas. *Phys. Rev. B* **1973**, *7*, 1912.

(34) Rajagopal, A. Inhomogeneous Relativistic Electron Gas. *J. Phys. C Solid State Phys.* **1978**, *11*, L943.

(35) MacDonald, A. H.; Vosko, S. A Relativistic Density Functional Formalism. *J. Phys. C Solid State Phys.* **1979**, *12*, 2977.

(36) Engel, E. *Relativistic Density Functional Theory: Foundations and Basic Formalism*; Elsevier, 2002; Vol. 11; pp 523–621.

(37) Neugebauer, J.; Hickel, T. Density Functional Theory in Materials Science. *Wiley Interdiscip. Rev. Comput. Mol. Sci.* **2013**, *3*, 438–448.

(38) Saal, J. E.; Kirklin, S.; Aykol, M.; Meredig, B.; Wolverton, C. Materials Design and Discovery With High-Throughput Density Functional Theory: The Open Quantum Materials Database (OQMD). *Jom* **2013**, *65*, 1501–1509.

(39) Liao, C.; Zhu, M.; Jiang, D.-e.; Li, X. Manifestation of the Interplay between Spin–Orbit and Jahn–Teller Effects in Au_{25} Superatom UV-Vis Fingerprint Spectra. *Chem. Sci.* **2023**, *14*, 4666–4671.

(40) Van Mourik, T.; Bühl, M.; Gaigeot, M.-P. Density Functional Theory Across Chemistry Physics and Biology. 2014.

(41) Cole, D. J.; Hine, N. D. Applications of Large-Scale Density Functional Theory in Biology. *J. Phys. Condens. Matter* **2016**, *28*, 393001.

(42) Saue, T.; Helgaker, T. Four-Component Relativistic Kohn–Sham Theory. *J. Comput. Chem.* **2002**, *23*, 814–823.

(43) Ratcliff, L. E.; Mohr, S.; Huhs, G.; Deutsch, T.; Masella, M.; Genovese, L. Challenges in Large Scale Quantum Mechanical Calculations. *Wiley Interdiscip. Rev. Comput. Mol. Sci.* **2017**, *7*, e1290.

(44) Teale, A. M.; Helgaker, T.; Savin, A.; Adamo, C.; Aradi, B.; Arbuznikov, A. V.; Ayers, P. W.; Baerends, E. J.; Barone, V.; Calaminici, P., et al. DFT Exchange: Sharing Perspectives on the Workhorse of Quantum Chemistry and Materials Science. *Phys. Chem. Chem. Phys.* **2022**, *24*, 28700–28781.

(45) Burke, K. Perspective on Density Functional Theory. *J. Chem. Phys.* **2012**, *136*.

(46) Mohr, S.; Ratcliff, L. E.; Genovese, L.; Caliste, D.; Boulanger, P.; Goedecker, S.; Deutsch, T. Accurate and Efficient Linear Scaling DFT Calculations With Universal Applicability. *Phys. Chem. Chem. Phys.* **2015**, *17*, 31360–31370.

(47) Becke, A. D. A Multicenter Numerical Integration Scheme for Polyatomic Molecules. *J. Chem. Phys.* **1988**, *88*, 2547–2553.

(48) Pederson, M. R.; Jackson, K. A. Variational Mesh for Quantum-Mechanical Simulations. *Phys. Rev. B* **1990**, *41*, 7453.

(49) Stratmann, R. E.; Scuseria, G. E.; Frisch, M. J. Achieving Linear Scaling in Exchange-Correlation Density Functional Quadratures. *Chem. Phys. Lett.* **1996**, *257*, 213–223.

(50) van Wüllen, C. Spin Densities in Two-Component Relativistic Density Functional Calculations: Noncollinear versus Collinear Approach. *J. Comput. Chem.* **2002**, *23*, 779–785.

(51) Peralta, J. E.; Scuseria, G. E.; Frisch, M. J. Noncollinear magnetism in density functional calculations. *Phys. Rev. B* **2007**, *75*, 125119.

(52) Salek, P.; Helgaker, T.; Saue, T. Linear Response at the 4-component Relativistic Density-functional Level: Application to the Frequency-dependent Dipole Polarizability of Hg, AuH and PtH_2. *Chem. Phys.* **2005**, *311*, 187–201.

(53) Bast, R.; Jensen, H. J. A.; Saue, T. Relativistic Adiabatic Time-Dependent Density Functional Theory Using Hybrid Functionals and Noncollinear Spin Magnetization. *Int. J. Quant. Chem.* **2009**, *109*, 2091–2112.

(54) Bulik, I. W.; Scalmani, G.; Frisch, M. J.; Scuseria, G. E. Noncollinear Density Functional Theory Having Proper Invariance and Local Torque Properties. *Phys. Rev. B* **2013**, *87*, 035117.

(55) Egidi, F.; Sun, S.; Goings, J. J.; Scalmani, G.; Frisch, M. J.; Li, X. Two-Component Non-Collinear Time-Dependent Spin Density Functional Theory for Excited State Calculations. *J. Chem. Theory Comput.* **2017**, *13*, 2591–2603.

(56) Petrone, A.; Williams-Young, D. B.; Sun, S.; Stetina, T. F.; Li, X. An Efficient Implementation of Two-Component Relativistic Density Functional Theory with Torque-Free Auxiliary Variables. *Euro. Phys. J. B* **2018**, *91*, 169.

(57) Luo, S.; Rivalta, I.; Batista, V.; Truhlar, D. G. Noncollinear Spins Provide a Self-Consistent Treatment of the Low-Spin State of a Biomimetic Oxomanganese Synthetic Trimer Inspired by the Oxygen Evolving Complex of Photosystem II. *J. Phys. Chem. Lett.* **2011**, *2*, 2629–2633.

(58) Luo, S.; Truhlar, D. G. Noncollinear Spin States for Density Functional Calculations of Open-Shell and Multi-Configurational Systems: Dissociation of MnO and NiO and Barrier Heights of O3, BeH2, and H4. *J. Chem. Theory Comput.* **2013**, *9*, 5349–5355.

(59) Xu, X.; Yang, K. R.; Truhlar, D. G. Testing Noncollinear Spin-Flip, Collinear Spin-Flip, and Conventional Time-Dependent Density Functional Theory for Predicting Electronic

Excitation Energies of Closed-Shell Atoms. *J. Chem. Theory Comput.* **2014**, *10*, 2070–2084.

(60) Pu, Z.; Li, H.; Zhang, N.; Jiang, H.; Gao, Y.; Xiao, Y.; Sun, Q.; Zhang, Y.; Shao, S. Noncollinear Density Functional Theory. *Phys. Rev. Res.* **2023**, *5*, 013036.

(61) Williams-Young, D. B.; De Jong, W. A.; Van Dam, H. J.; Yang, C. On the Efficient Evaluation of the Exchange Correlation Potential on Graphics Processing Unit Clusters. *Front. Chem.* **2020**, *8*, 581058.

(62) Nitsche, M. A.; Ferreria, M.; Mocskos, E. E.; Gonzalez Lebrero, M. C. GPU Accelerated Implementation of Density Functional Theory for Hybrid QM/MM Simulations. *J. Chem. Theory Comput.* **2014**, *10*, 959–967.

(63) Manathunga, M.; Miao, Y.; Mu, D.; Goötz, A. W.; Merz Jr, K. M. Parallel Implementation of Density Functional Theory Methods in the Quantum Interaction Computational Kernel Program. *J. Chem. Theory Comput.* **2020**, *16*, 4315–4326.

(64) Williams-Young, D. B.; Asadchev, A.; Popovici, D. T.; Clark, D.; Waldrop, J.; Windus, T. L.; Valeev, E. F.; de Jong, W. A. Distributed Memory GPU Accelerated Fock Construction for Hybrid Gaussian Basis Density Functional Theory. *J. Chem. Phys.* **2023**, *158*.

(65) Gross, a. E.; Dobson, J.; Petersilka, M. Density Functional Theory of Time-Dependent Phenomena. *Density Funct. Theory Ii Relativistic Time Depend. Ext.* **2005**, 81–172.

(66) Runge, E.; Gross, E. K. Density-Functional Theory for Time-Dependent Systems. *Phys. Rev. Lett.* **1984**, *52*, 997.

(67) Marques, M. A.; Gross, E. K. Time-Dependent Density Functional Theory. *Annu. Rev. Phys. Chem.* **2004**, *55*, 427–455.

(68) Goings, J. J.; Lestrange, P. J.; Li, X. Real-Time Time-Dependent Electronic Structure Theory. *WIREs Comput. Mol. Sci.* **2018**, *8*, e1341.

(69) Li, X.; Govind, N.; Isborn, C.; DePrince, A. E.; Lopata, K. Real-Time Time-Dependent Electronic Structure Theory. *Chem. Rev.* **2020**, *120*, 9951–9993.

(70) Dyall, K. G.; Enevoldsen, T. Interfacing Relativistic and Nonrelativistic Methods. III. Atomic 4-Spinor Expansions and Integral Approximations. *J. Chem. Phys.* **1999**, *111*, 10000–10007.

(71) Dyall, K. G. Interfacing Relativistic and Nonrelativistic Methods. IV.. One- and Two-Electron Scalar Approximations. *J. Chem. Phys.* **2001**, *115*, 9136–9143.

(72) Peng, D.; Liu, W.; Xiao, Y.; Cheng, L. Making Four- and Two-Component Relativistic Density Functional Methods Fully Equivalent Based on the Idea of From Atoms to Molecule. *J. Chem. Phys.* **2007**, *127*, 104106.

(73) Liu, W.; Peng, D. Exact Two-component Hamiltonians Revisited. *J. Chem. Phys.* **2009**, *131*, 031104.

(74) Liu, W. Ideas of Relativistic Quantum Chemistry. *Mol. Phys.* **2010**, *108*, 1679–1706.

(75) Li, Z.; Xiao, Y.; Liu, W. On the Spin Separation of Algebraic Two-Component Relativistic Hamiltonians. *J. Chem. Phys.* **2012**, *137*, 154114.

(76) Peng, D.; Middendorf, N.; Weigend, F.; Reiher, M. An Efficient Implementation of Two-Component Relativistic Exact-Decoupling Methods for Large Molecules. *J. Chem. Phys.* **2013**, *138*, 184105.

(77) Egidi, F.; Goings, J. J.; Frisch, M. J.; Li, X. Direct Atomic-Orbital-Based Relativistic Two-Component Linear Response Method for Calculating Excited-State Fine Structures. *J. Chem. Theory Comput.* **2016**, *12*, 3711–3718.

(78) Goings, J. J.; Kasper, J. M.; Egidi, F.; Sun, S.; Li, X. Real Time Propagation of the Exact Two Component Time-Dependent Density Functional Theory. *J. Chem. Phys.* **2016**, *145*, 104107.

(79) Konecny, L.; Kadek, M.; Komorovsky, S.; Malkina, O. L.; Ruud, K.; Repisky, M. Acceleration of Relativistic Electron Dynamics by Means of X2C Transformation: Application to the Calculation of Nonlinear Optical Properties. *J. Chem. Theory Comput.* **2016**, *12*, 5823–5833.

(80) Liu, J.; Cheng, L. Relativistic Coupled-Cluster and Equation-of-Motion Coupled-Cluster Methods. *WIREs Comput. Mol. Sci.* **2021**, *11*, 1536.

(81) Sharma, P.; Jenkins, A. J.; Scalmani, G.; Frisch, M. J.; Truhlar, D. G.; Gagliardi, L.; Li, X. Exact-Two-Component Multiconfiguration Pair-Density Functional Theory. *J. Chem. Theory Comput.* **2022**, *18*, 2947–2954.

(82) Lu, L.; Hu, H.; Jenkins, A. J.; Li, X. Exact-Two-Component Relativistic Multireference Second-Order Perturbation Theory. *J. Chem. Theory Comput.* **2022**, *18*, 2983–2992.

(83) Hoyer, C. E.; Hu, H.; Lu, L.; Knecht, S.; Li, X. Relativistic Kramers-Unrestricted Exact-Two-Component Density Matrix Renormalization Group. *J. Phys. Chem. A* **2022**, *126*, 5011–5020.

(84) Ehrman, J.; Martinez-Baez, E.; Jenkins, A. J.; Li, X. Improving One-Electron Exact-Two-Component Relativistic Methods with the Dirac–Coulomb–Breit-Parameterized Effective Spin–Orbit Coupling. *J. Chem. Theory Comput.* **2023**, *19*, 5785–5790.

(85) Zhang, T.; Banerjee, S.; Koulias, L. N.; Valeev, E. F.; DePrince, A. E. I.; Li, X. Dirac–Coulomb–Breit Molecular Mean-Field Exact-Two-Component Relativistic Equation-of-Motion Coupled-Cluster Theory. *J. Phys. Chem. A* **2024**, *128*, 3408–3418.

(86) Boettger, J. C. Approximate Two-Electron Spin-Orbit Coupling Term For Density-Functional-Theory DFT Calculations Using The Douglas-Kroll-Hess Transformation. *Phys. Rev. B* **2000**, *62*, 7809–7815.

(87) Williams-Young, D. B.; de Jong, W. A.; van Dam, H. J.; Yang, C. On the Efficient Evaluation of the Exchange Correlation Potential on Graphics Processing Unit Clusters. *Front. Chem.* **2020**, *8*, 581058.

(88) Williams-Young, D. B.; Bagusetty, A.; de Jong, W. A.; Doerfler, D.; van Dam, H. J.; Vázquez-Mayagoitia, Á.; Windus, T. L.; Yang, C. Achieving Performance Portability in Gaussian Basis Set Density Functional theory on accelerator based architectures in NWChemEx. *Parallel Comput.* **2021**, *108*, 102829.

(89) Williams-Young, D. B.; Petrone, A.; Sun, S.; Stetina, T. F.; Lestrange, P.; Hoyer, C. E.; Nascimento, D. R.; Koulias, L.; Wildman, A.; Kasper, J.; Goings, J. J.; Ding, F.; DePrince III, A. E.; Valeev, E. F.; Li, X. The Chronus Quantum (ChronusQ) Software Package. *WIREs Comput. Mol. Sci.* **2020**, *10*, e1436.

(90) Chatzigoulas, A.; Karathanou, K.; Dellis, D.; Cournia, Z. NanoCrystal: A Web-Based Crystallographic Tool for the Construction of Nanoparticles Based on Their Crystal Habit. *J. Chem. Inf. Model.* **2018**, *58*, 2380–2386.

(91) Persson, K. Materials Data on Cu (SG:225) by Materials Project. 2016.

(92) Persson, K. Materials Data on Au (SG:225) by Materials Project. 2016.

(93) Persson, K. Materials Data on Ag (SG:225) by Materials Project. 2014.

(94) Perdew, J. P.; Burke, K.; Ernzerhof, M. Generalized Gradient Approximation Made Simple. *Phys. Rev. Lett.* **1996**, *77*, 3865–3868.

(95) Perdew, J. P.; Burke, K.; Ernzerhof, M. Generalized Gradient Approximation Made Simple [Phys. Rev. Lett. 77, 3865 (1996)]. *Phys. Rev. Lett.* **1997**, *78*, 1396–1396.

TOC Graphic